Structure and Dynamics of 3,5-Di-tert-butylpyrazole Probed by Combined X-ray Crystallography and 15N Solid State NMR

ARTICLE *in* THE JOURNAL OF ORGANIC CHEMISTRY · APRIL 1995

Impact Factor: 4.72 · DOI: 10.1021/jo00112a015

6 AUTHORS, INCLUDING:

Hans-Heinrich Limbach
Freie Universität Berlin
333 PUBLICATIONS **8,990** CITATIONS
SEE PROFILE

Nadine Jagerovic
Spanish National Research Council
125 PUBLICATIONS **1,607** CITATIONS
SEE PROFILE

José Elguero
Spanish National Research Council
1,502 PUBLICATIONS **22,232** CITATIONS
SEE PROFILE

Structure and Dynamics of 3,5-Di-*tert*-butylpyrazole Probed by Combined X-ray Crystallography and ^{15}N Solid State NMR

Francisco Aguilar-Parrilla,[†] Hans-Heinrich Limbach,*[,†] Concepción Foces-Foces,*[,‡] Félix Hernández Cano,[‡] Nadine Jagerovic,[§] and José Elguero*[,§]

Institut für Organische Chemie, Freie Universität Berlin, Takustr. 3, D-14195 Berlin, F.R.G., Departamento de Cristalografía, Instituto de Química-Física "Rocasolano", CSIC, Serrano 119, E-28006 Madrid, Spain, and Instituto de Química Médica, CSIC, Juan de la Cierva 3, E-28006 Madrid, Spain

Received December 17, 1993 (Revised Manuscript Received January 27, 1995[⊗])

The crystal structure of the title compound was determined by X-ray crystallography: $C_{11}H_{20}N_2$, *Pbca*, $Z = 8$, $a = 11.4779(3)$, $b = 21.1004(1)$, $c = 9.9801(2)$ Å, $D_x = 0.99$ g cm^{-3}. The results show that crystals of 3,5-di-*tert*-butylpyrazole are formed by three types of dimers AA, AB or BA, and BB differing in the conformation of the *tert*-butyl groups. Variable temperature ^{15}N-CPMAS-NMR experiments which were carried out on a solid ^{15}N-labeled sample indicate a conformational interconversion of the different dimers via *tert*-butyl group rotation as well as a nondegenerate intradimer double proton transfer. The rate and equilibrium constants of the tautomerism were obtained by ^{15}N-CPMAS-NMR line-shape analysis. These constants represent averages of the different conformational states. The analysis of the data suggests that the tautomerism takes place only in the symmetric conformer AA where the tautomerism is degenerate. The observed nondegeneracy is then not the consequence of solid state effects, but of the intrinsic conformational exchange.

1. Introduction

Pyrazoles constitute a very interesting class of heterocyclic compound despite their simple structure in the gas phase.[1] A large variety of hydrogen bonded complexes was found to be present in the solid state, depending on the substituents of the pyrazole ring.[2-7] Whereas the parent pyrazole compound forms linear hydrogen bonded chains in the solid state where proton tautomerism is suppressed[8-10] (See Figure 1), unexpected and remarkable changes in the crystal structure occur when substituents are introduced at the carbon atoms C3, C4, and C5 of the pyrazole ring. In addition, intermolecular proton transfer processes in these pyrazole complexes were detected for the first time by ^{13}C- and in particular, by ^{15}N-CPMAS-NMR spectroscopy (CP: cross polarization, MAS: magic angle spinning).[2-7] For example, in the case of the symmetric substituted 3,5-dimethylpyrazole (DMP), cyclic hydrogen bonded trimers are formed in the solid state where a correlated degenerate triple proton transfer takes place as shown in Figure 1.[2,3] By combining X-ray crystallography with ^{15}N-CPMAS-NMR spectroscopy, the crystal structure and proton tautomerism were fully characterized.[2-3]

Further X-ray crystallographic investigations showed that a cyclic tetramer formed when the methyl groups in the DMP were replaced by phenyl rings leading to the 3,5-diphenylpyrazole compound (DPP). When, in addition, a bromine atom is finally introduced at position 4 of the DPP, a dimer results (3,5-diphenyl-4-bromopyrazole = DPBrP). In both compounds degenerate proton transfers were again detected by ^{15}N-CPMAS-NMR spectroscopy (see Figure 1).[4,5]

In contrast, asymmetric substitution of the pyrazole ring with nitro,[11] hydroxymethyl,[12] and carboxy groups,[13] or other pyrazole rings[14] leads to a suppression of the solid state proton tautomerism.

The question then arises as to how chemically identical substituents which can also adopt different conformations affect the tautomerism. In order to study this problem we chose 3,5-di-*tert*-butylpyrazole (DTBUP) as a model compound because of the variable dihedral angles between the pyrazole ring and the methyl groups (see Figure 2). If this angle is different for both *tert*-butyl groups, one could expect a perturbation of the gas phase degeneracy of the proton tautomerism. Since *tert*-butyl groups may rotate in solid organic compounds,[15] an influence of this rotation on the proton tautomerism could be the consequence.

[†] Freie Universität Berlin.
[‡] Instituto "Rocasolano".
[§] Instituto de Química Médica.
[⊗] Abstract published in *Advance ACS Abstracts,* March 15, 1995.

(1) Elguero, J. In *Comprehensive Heterocyclic Chemistry*; Katritzky, A. R., Rees, C. W., Eds.; Pergamon Press: Oxford, 1984; pp 167–303.
(2) Baldy, A.; Elguero, J.; Faure, R.; Pierrot, M.; Vincent, E. J. *J. Am. Chem. Soc.* **1985**, *107*, 5290–5291.
(3) Smith, J. A. S.; Wehrle, B.; Aguilar-Parrilla, F.; Limbach, H.-H.; Foces-Foces, C.; Cano, F. H.; Elguero, J.; Baldy, A.; Pierrot, M.; Khurshid, M. M. T.; Larcombe-McDouall, J. B. *J. Am. Chem. Soc.* **1989**, *111*, 7304–7312.
(4) Aguilar-Parrilla, F.; Scherer, G.; Limbach, H.-H.; Foces-Foces, C.; Cano, F. H.; Smith, J. A. S.; Toiron, C.; Elguero, J. *J. Am. Chem. Soc.* **1992**, *114*, 9657–9659.
(5) Elguero, J.; Cano, F. H.; Foces-Foces, C.; Llamas-Saiz, A. L.; Limbach, H.-H.; Aguilar-Parrilla, F.; Claramunt, R. M.; López, C. *J. Heterocycl. Chem.* **1994**, *31*, 695–700.
(6) Toda, F.; Tanaka, K.; Foces-Foces, C.; Llamas-Saiz, A. L.; Limbach, H.-H.; Aguilar-Parrilla, F.; Claramunt, R. M.; López, C.; Elguero, J. *J. Chem. Soc. Chem. Commun.* **1993**, 1139–1142.
(7) Aguilar-Parrilla, F.; Claramunt, R. M.; López, C.; Sanz, D.; Limbach, H.-H.; Elguero, J. *J. Phys. Chem.* **1994**, *98*, 8752–8760.
(8) Ehrlich, H. W. W. *Acta Crystallogr.* **1960**, *13*, 946.
(9) Berthou, J.; Elguero, J.; Rérat, C. *Acta Crystallogr. Sect. B* **1970**, *26*, 1881–1882.
(10) Larsen, F. K.; Lehmann, M. S.; Sotofte, I.; Rasmussen, S. E. *Acta Chem. Scand.* **1970**, *24*, 3248–3258.
(11) Foces-Foces, C.; Cano, F. H.; Elguero, J. *Gazz. Chim. Ital.* **1993**, *123*, 477–479.
(12) Llamas-Saiz, A. L.; Foces-Foces, C.; Elguero, J.; Meutermans, W. *Acta Crystallogr.* **1992**, *C48*, 714–717.
(13) Llamas-Saiz, A. L.; Foces-Foces, C.; Elguero, J.; Meutermans, W. *Supramolec. Chem.* **1994**, *4*, 53–62.
(14) Monge, M. A.; Gutierrez-Puebla, E.; Elguero, J.; Toiron, C.; Meutermans, W.; Sobrados, I. *Spectrochim. Acta* **1994**, *50A*, 727–734.
(15) Riddell, F. G.; Arumugam, S.; Harris, K. D. M.; Rogerson, M.; Strange, J. H. *J. Am. Chem. Soc.* **1993**, *115*, 1881–1885.

0022-3263/95/1960-1965$09.00/0

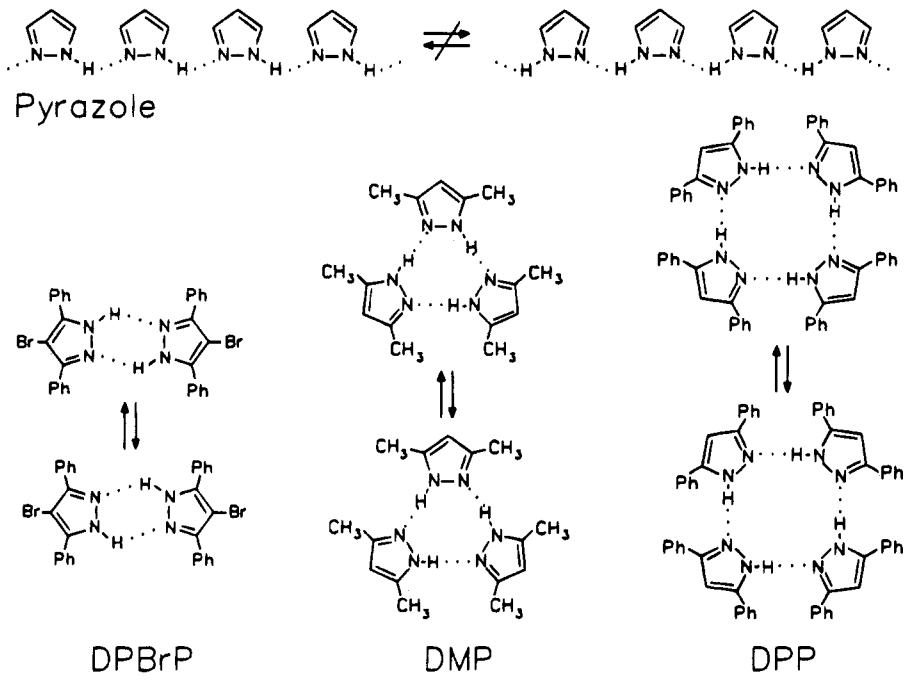

Figure 1. Schematic structures of some pyrazole derivatives in the solid state.

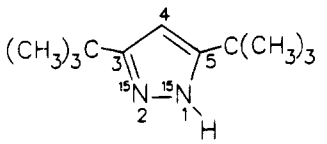

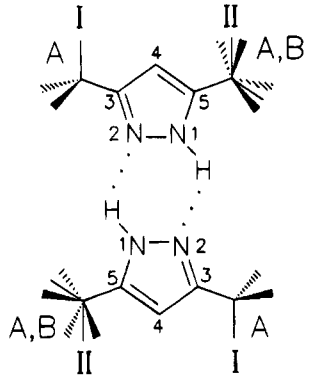

Figure 2. Average structure of DTBUP as determined by X-ray crystallography showing the conformation A of the *tert*-butyl group of category I and the two possible conformations A and B of the *tert*-butyl groups of category II.

In the following, we report the results of a combined X-ray crystallographic and ^{15}N-CPMAS-NMR spectroscopic study of solid DTBUP. For the NMR measurements, DTBUP was enriched with the ^{15}N isotope. We will show that only the combination of both analytical methods leads to a proper description of the complex exchange processes in solid DTBUP.

2. Experimental Section

Synthesis of Labeled $^{15}N_2$-3,5-Di-*tert*-butylpyrazole (DTBUP). DTBUP was prepared from dipivaloylmethane and hydrazine according to the described procedure.[16] Suitable crystals for the structural study were obtained by slow evaporation of a saturated ethanol solution. The double labeled compound was prepared in a similar way using $^{15}NH_2{}^{15}NH_2$.

Table 1. Final Atomic Coordinates[a]

atom	*x*	*y*	*z*
N2	0.4742(3)	0.0737(2)	0.5400(3)
N1	0.4037(3)	0.0464(2)	0.4463(3)
C5	0.3187(4)	0.0860(2)	0.4079(4)
C4	0.3339(4)	0.1416(2)	0.4798(5)
C3	0.4326(4)	0.1317(2)	0.5602(4)
C6	0.2300(4)	0.0674(2)	0.3046(5)
C7	0.4895(4)	0.1764(2)	0.6583(5)
*C8	0.1423(14)	0.1247(9)	0.2875(19)
*C9	0.1817(27)	0.0052(11)	0.3292(34)
*C10	0.2843(15)	0.0648(18)	0.1665(16)
C11	0.4166(7)	0.2374(3)	0.6722(10)
C12	0.6081(7)	0.1964(5)	0.6004(11)
C13	0.5029(17)	0.1464(4)	0.7908(8)
*C8 P	0.1153(12)	0.0658(21)	0.3695(24)
*C9 P	0.2417(22)	0.1098(11)	0.1865(21)
*C10 P	0.2620(18)	−0.0038(10)	0.2535(21)

[a] pp(C8)= pp(C9)= pp(C10)= 0.57(4), pp(C8P)= pp(C9)= pp(C10P)= 0.43(4).

X-ray Crystallography.[24] $C_{11}H_{20}N_2$, M = 180.29, *Pbca*, Z = 8, a = 11.4779(3), b = 21.1004(1), c = 9.9801(2) Å, D_x = 0.99 g cm^{-3}. Philips PW1100 diffractometer, Cu Kα radiation. The structure was solved by direct methods[17] and refined by full matrix least-squares procedures[18]. $R(Rw)$ = 0.110 (0.127) for 1338 observed reflections [$I > 3\sigma(I)$]. Peaks higher than 0.36 e Å^{-3} were not found in the final difference synthesis. The final atomic coordinates for the non-hydrogen atoms are listed in Table 1. Selected geometrical parameters are listed in Table 2.

^{15}N-CPMAS-NMR Spectroscopy. The ^{15}N-CPMAS-NMR spectra were recorded on a Bruker CXP 100 spectrometer

(16) Elguero, J.; Gonzalez, E.; Jacquier, R. *Bull. Soc. Chim. Fr.* **1968**, 707–713.
(17) Stewart, J. M.; Machin, P. A.; Dickinson, C. W.; Ammon, H. L.; Heck, H.; Flack, H. *The X-Ray System*; Technical Report TR-446, Computer Science Center, Univ. of Maryland (1980).
(18) Burla, M. C.; Camalli, M.; Cascarano, G.; Giacovazzo, G.; Polidori, G.; Spagna, R.; Viterbo, D. *J. Appl. Crystallogr.* **1989**, *22*, 389–393.

Table 2. Selected Geometrical Parameters (Å, deg)

N2–N1	1.364(5)	C6–C9	1.445(25)
N2–C3	1.328(5)	C6–C10	1.513(27)
N1–C5	1.340(5)	C6–C8P	1.467(17)
C5–C4	1.386(6)	C6–C9P	1.486(22)
C5–C6	1.501(7)	C6–C10P	1.629(22)
C4–C3	1.404(6)	C7–C11	1.542(9)
C3–C7	1.509(6)	C7–C12	1.537(10)
C6–C8	1.582(18)	C7–C13	1.473(10)
N1–N2–C3	106.2(3)	C5–C6–C8P	108.2(10)
N2–N1–C5	111.4(3)	C5–C6–C10	110.8(8)
N1–C5–C6	121.9(4)	C5–C6–C9	112.4(12)
N1–C5–C4	106.7(4)	C5–C6–C8	107.8(8)
C4–C5–C6	131.5(4)	C3–C7–C13	111.0(5)
C5–C4–C3	105.8(4)	C3–C7–C12	108.2(5)
N2–C3–C4	109.9(4)	C3–C7–C11	110.2(5)
C4–C3–C7	128.9(4)	C12–C7–C13	111.3(7)
N2–C3–C7	121.2(4)	C11–C7–C13	109.5(6)
C5–C6–C10P	107.6(8)	C11–C7–C12	106.5(5)
C5–C6–C9P	109.0(10)		
N1–C5–C6–C8	178.6(8)	N1–C5–C6–C10P	−1.6(9)
N1–C5–C6–C9	47.0(14)	N2–C3–C7–C11	−174.4(5)
N1–C5–C6–C10	−71.7(12)	N2–C3–C7–C12	69.5(6)
N1–C5–C6–C8P	115.5(13)	N2–C3–C7–C13	−52.9(8)
N1–C5–C6–C9P	−117.0(10)		

working at 90.02 MHz for protons and 9.12 MHz for ^{15}N. The spectrometer was equipped with a 7 mm CPMAS probehead from Doty Scientific, USA. The spinning speeds were of the order of 2–3 kHz. A Bruker B VT 1000 temperature unit was used to control the temperature of the bearing nitrogen gas stream, and a homebuilt heat exchanger was employed in order to achieve low temperatures. Standard one-dimensional CPMAS-NMR experiments[19] were performed. General recording parameters: quadrature detection, 5.5 μs ^{1}H-90° pulse width, 2–8 ms CP times, 4 s recycle delay, spectral width of 7000 Hz, line broadening of 20 Hz. All ^{15}N chemical shifts are related to external solid $^{15}NH_4Cl$.

3. Results

X-ray Crystallography. The results of the crystallographic measurements performed on DTBUP are assembled in Tables 1 and 2 and depicted in Figure 3. DTBUP crystallizes in the *Pbca* space group with $Z = 8$ molecules in the unit cell. These molecules form four pairs of cyclic dimers which are quasiequivalent if variations of the conformation of the *tert*-butyl groups and effects of tautomerism are neglected. A careful analysis of the data reveals that there is either a static, or a dynamic disorder, with respect to both the conformation of the *tert*-butyl groups and to proton tautomerism. There are two categories (I and II) of *tert*-butyl group. In category I the *tert*-butyl groups are ordered and adopt a conformation labeled as A, where one methyl group points toward the 4-CH group (Figure 2). In other words, there are only three possible positions for the methyl groups of these *tert*-butyl groups.

By contrast, there are six positions for the methyl groups of the *tert*-butyl groups of category II. The situation can best be described as a superposition of *tert*-butyl groups in conformation A and in another, conformation B, where one methyl group points toward the nitrogen atom (Figure 2). The best data fit is obtained with a value of $x_A = 1 - x_B = 0.60 \pm 0.04$, where x_A and x_B represent the mole fractions of conformations A and B in category II. In other words, the *tert*-butyl groups of category II are "disordered". The X-ray crystallographic data indicate that each molecule contains *tert*-butyl groups of both categories and that these are diagonally arranged in the cyclic dimers as illustrated in Figure 4. Furthermore, a partial disorder of the mobile protons is observed. It appears that the latter are dominantly located on the nitrogen atoms close to the *tert*-butyl groups of category II. The average mole fraction of protonated nitrogen atoms near *tert*-butyl groups of category II was found to be approximately $x_{II} = 1 - x_I = 0.9$.

By X-ray crystallography it is not possible to decide whether the conformational *tert*-butyl group disorder and the proton disorder in the hydrogen bonds is static or dynamic. In the first case, the structure of a given molecule is time independent but varies from one unit cell to the other. In the case of a dynamic disorder, each molecule experiences time dependent structural changes. It follows that, a priori, one has to consider all six different combinations concerning the position of the mobile protons and the conformation of *tert*-butyl groups of category II as illustrated in Figure 4. The different species may be characterized by AA(1), AA(2), AB(1), etc. with the corresponding molefractions $x_{AA(1)}$, $x_{AA(2)}$, $x_{AB(1)}$ etc.; where the double capital letters notation refers to the conformation of the two *tert*-butyl groups of category II. Tautomers AA(1), AB(1), and BB(1) seem to be favored over the tautomers AA(2), AB(2) and BB(2). In the case of the AA dimer, the asymmetry is absent in the gas phase but can be induced in the solid state by intermolecular interactions. In other words, the three proton transfer steps in Figure 4 could also involve three different equilibrium constants, i.e. three different forward and backward rate constants.

^{15}N-CPMAS-NMR Spectroscopy. Since X-ray crystallography cannot give detailed information on the exchange processes of Figure 4 we measured the ^{15}N-CPMAS-NMR spectra of $^{15}N_2$ labeled DTBUP as a function of temperature as shown in Figure 5. At 252 K only two signals were observed at 241 and 159.5 ppm. The low-field signal rises from the nonprotonated nitrogen atoms, the high-field line from the corresponding protonated nitrogen neighbors. This assignment was corroborated in a dipolar dephasing experiment[20] in which only the low-field line survived. We noted that the low-field line was substantially broader than the high-field one. This effect was found to be reproducible and was not caused by instrumental artifacts such as a deviation of the sample spinning axis from the magic angle. Therefore, this effect can be explained by the presence of two unresolved low-field signals as expected for two different, slowly exchanging nonprotonated nitrogen atoms experiencing different *tert*-butyl group conformations A or B. The influence of these conformations on the chemical shift of the protonated nitrogen atoms is less pronounced, leading to a differential line width of the two signals at low temperature.[21] At higher temperatures the differential line width disappears. Knowing the X-ray results presented above, we can easily explain this effect in terms of a *tert*-butyl group rotation between conformations A and B, which is then faster than the chemical shift difference of the nonprotonated nitrogen atoms. In addition, the proton transfer is also activated at this temperature as can be inferred from the broadening of

(19) Fyfe, C. A. *Solid State NMR for Chemists*; CFC Press: Guelph, Ontario, 1983.

(20) Opella, S. J.; Frey, M. H. *J. Am. Chem. Soc.* **1979**, *101*, 5854–5856.

(21) Aguilar-Parrilla, F.; Männle, F.; Limbach, H.-H.; Jagerovic, N.; Elguero, J. *Magn. Reson. Chem.* **1994**, *32*, 699–702.

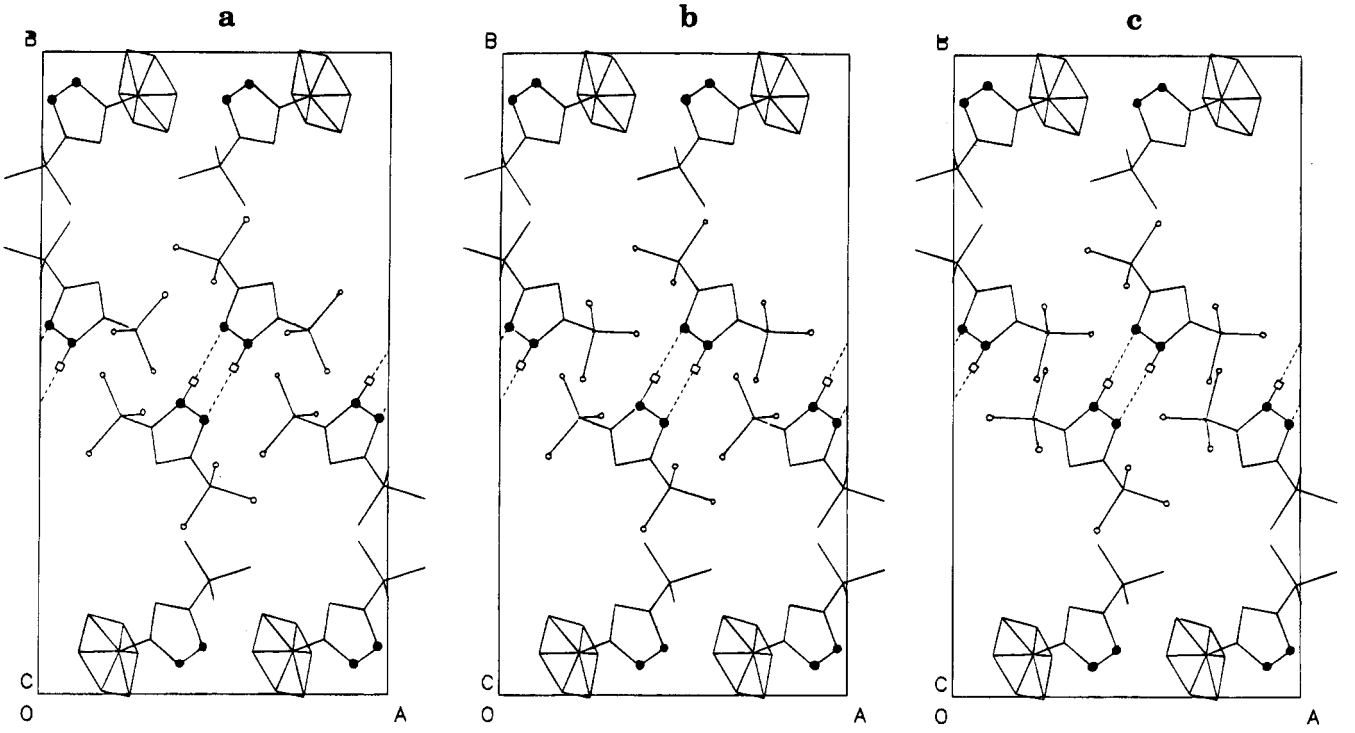

Figure 3. Packing diagram of the three dimers of DTBUP (black dots: nitrogen atoms, white dots: methyl groups): (a) AA, (b) AB or BA, (c) BB.

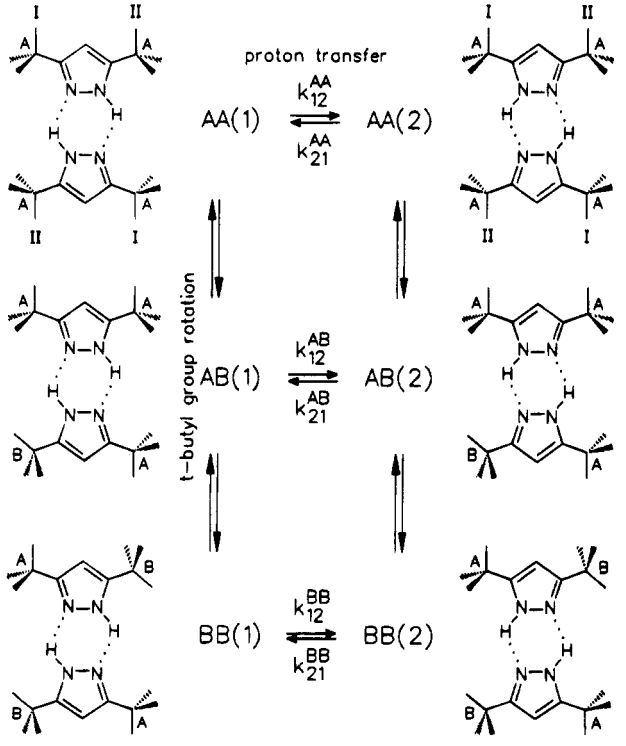

Figure 4. Possible reaction network of DTBUP in the case of a dynamic proton transfer and *tert*-butyl group rotation in the three different dimers (for further explanation see text).

the NH line. As the temperature is raised, both lines broaden, sharpen and move toward each other but do not coalesce, completely characteristic for a nondegenerate proton exchange between two unequally populated states **1** and **2**.[22,23] At a high temperature, the two lines are slightly broader than at a low temperature. This effect could either arise from a distribution of equilibrium constants of tautomerism and/or from an interference of various molecular motions with MAS and ^{1}H decoupling.[19] The two lines also exhibit slightly different intensities which arise from different cross polarization dynamics at a high temperature. The spectra only depend on the chemical shifts ν_N and ν_{NH} of the nonprotonated and protonated nitrogen atoms, the line width W_0 in the absence of proton exchange and the rate and equilibrium constants k_{12} and $K_{12} = k_{12}/k_{21} = x_2/x_1$. These represent averages of the varying conformations of Figure 4.

From the line splittings $\delta\nu$ at high temperature and the low temperature splitting $\Delta\nu = \nu_N - \nu_{NH}$, the equilibrium constants K_{12} (Table 3) can be obtained using the following equation:[22,23]

$$K_{12} = x_{AA_2}/x_{AA_1} = (1 - \delta\nu/\Delta\nu)/(1 + \delta\nu/\Delta\nu). \quad (1)$$

The van't Hoff plot is linear as shown in Figure 6a. At room temperature (298 K) an equilibrium constant of $K_{12} = 0.163$ was found corresponding to 86% of the major tautomer **1**. By linear regression, a reaction enthalpy of $\Delta H_{12} = 7.7$ kJ mol^{-1} and a reaction entropy of $\Delta S_{12} = 10.8$ J K^{-1} mol^{-1} were obtained.

The results of the line-shape analysis were extremely satisfactory as can be inferred from Figure 5. The spectra were calculated assuming two, two-site systems with different —N= and same —NH chemical shifts. The forward rate constants obtained for the tautomerism

(22) Wehrle, B.; Zimmermann, H.; Limbach, H.-H. *J. Am. Chem. Soc.* **1988**, *110*, 7014–7024.

(23) (a) Limbach, H.-H.; Wehrle, B.; Zimmermann, H.; Kendrick, R. D.; Yannoni, C. S. *J. Am. Chem. Soc.* **1987**, *109*, 929–930. (b) Limbach, H.-H.; Wehrle, B.; Zimmermann, H.; Kendrick, R. D.; Yannoni, C. S. *Angew. Chem. Int. Ed. Engl.* **1987**, *26*, 247–249.

(24) The author has deposited atomic coordinates for this structure with the Cambridge Crystallographic Data Centre. The coordinates can be obtained, on request, from the Director, Cambridge Crystallographic Data Centre, 12 Union Road, Cambridge, CB2 1EZ, UK.

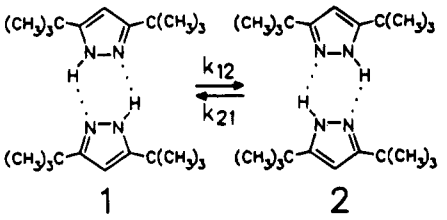

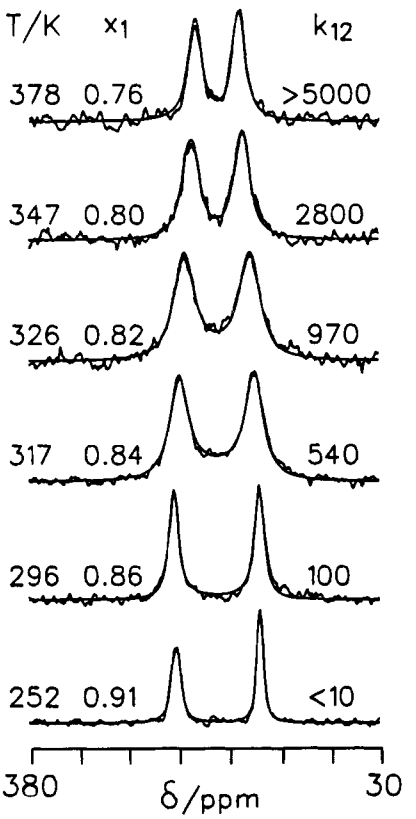

Figure 5. 9.12 MHz superposed variable temperature experimental and calculated ^{15}N-CPMAS-NMR spectra of DTBUP. Sweep width of 7000 Hz, CP-times of 2–8 ms, average scan number of 500; x_1 being the molar fraction of the dominating tautomer, k_{12} the forward rate constant.

Table 3. Temperature Dependence of the Equilibrium Constant K_{12} Obtained by Linear Regression of the Obtained Data, x_1 Being the Molar Fraction of the Dominating Tautomer, k_{12} the Forward Rate Constant Obtained by Line-Shape Analysis

T, K	K_{12}	x_1	k_{12}, s^{-1}
252	0.092	0.91	<10
296	0.159	0.86	100
307	0.178	0.85	230
317	0.196	0.84	540
326	0.213	0.82	970
338	0.236	0.81	1900
347	0.253	0.80	2800
378	0.315	0.76	>5000

(Table 3) can be expressed by the equation:

$$k_{12} = k_{21}/K_{12} \approx 10^{12} \exp(-56.6 \text{ kJ mol}^{-1}/RT). \quad (2)$$

The corresponding Arrhenius plot is shown in Figure 6b.

4. Discussion

From the X-ray results presented in the previous section it was concluded that DTBUP forms four cyclic

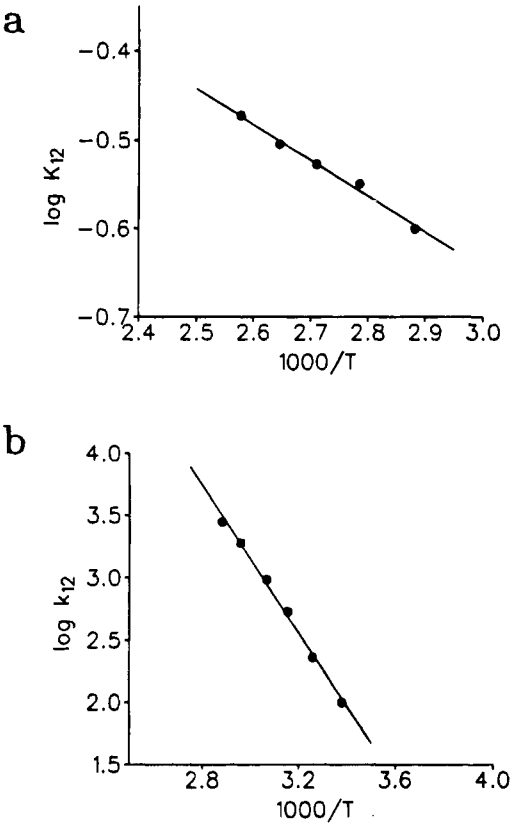

Figure 6. (a) Van't Hoff diagram showing the temperature dependence of the equilibrium constant K_{12} of the asymmetric proton transfer process in DTBUP. (b) Arrhenius diagram of the asymmetric double proton transfer in DTBUP.

dimers in the unit cell differing in the conformation of the *tert*-butyl groups in position II as shown in Figure 2. According to the latter, one can formulate three different types of dimer: AA, AB, and BB, as shown in Figure 4. Via X-ray analysis, however, it was not possible to decide whether the average structure determined and shown in Figure 2 was due to a static or a dynamic disorder. In addition, a disorder in the mobile proton sites was detected. Again, it was not possible to decide between a static or a dynamic disorder. If a dynamic disorder is present in both cases, one can formulate, a priori, the reaction network shown in Figure 4 where all three dimer types interchange through rotation of the *tert*-butyl groups and proton transfer.

By ^{15}N-CPMAS-NMR spectroscopy, evidence was obtained for such a dynamic disorder in the *tert*-butyl groups and in the mobile proton sites as depicted in Figure 5. It was also found that the exchange rates between the various conformers in Figure 4 are of the same order as those of the proton tautomerism. If the exchange between the conformers was slow, the ^{15}N NMR spectra would be characterized by three equilibrium constants and six rate constants and as a consequence, six lines should be present at high temperature, but this is not the case. Nevertheless, the NMR spectra could be simulated in terms of a single averaged species interconverting between the tautomeric states 1 and 2. Therefore, the observed quantities for the rate constants k_{12} and the equilibrium constants K_{12} represent averages of all the conformations, thus, depending on the individual rate and equilibrium constants leading to a nonlinear Arrhenius or van't Hoff curves. If the rate and equilibrium constants of the proton transfer in the three

Table 4. Selected Geometric Parameters of the Hydrogen Bonds in DTBUP and DPBrP

compound	N···N [Å]	N−H···N [deg]	space group
DTBUP	2.90	149	*Pbca*
DPBrP	2.836	138	$P\bar{1}$

conformers of Figure 4 are equal, i.e. not affected by the conformation of the *tert*-butyl groups, it follows that

$$\bar{k}_{12} = k_{12}^{\mathrm{AA(1)\rightarrow AA(2)}} = k_{12}^{\mathrm{AB(1)\rightarrow AB(2)}} = k_{12}^{\mathrm{BB(1)\rightarrow BB(2)}} \quad (3)$$

and

$$\bar{K}_{12} = K_{12}^{\mathrm{AA(1)\rightarrow AA(2)}} = K_{12}^{\mathrm{AB(1)\rightarrow AB(2)}} = K_{12}^{\mathrm{BB(1)\rightarrow BB(2)}} \quad (4)$$

In the second case where the tautomerism of AA is degenerate and AB and BB suppressed, i.e. $k_{12}^{\mathrm{AB}} = k_{12}^{\mathrm{BB}} = 0$, $x_{\mathrm{AB(2)}} = x_{\mathrm{BB(2)}} = 0$ and $k_{12}^{\mathrm{AA}} = k_{21}^{\mathrm{AA}}$ we obtain

$$k_{12} = k_{12}^{\mathrm{AA}} K_{12} \quad (5)$$

and

$$K_{12} = \frac{1}{1 + K_{\mathrm{AA\rightarrow AB}} + K_{\mathrm{AA\rightarrow AB}} K_{\mathrm{AB\rightarrow BA}}} \quad (6)$$

In principle, the experimental Arrhenius and van't Hoff curves log k_{12} and log K_{12} vs $1/T$ should be slightly nonlinear. However, a very large temperature range is required in order to detect such a nonlinearity, so the experimental data expressed by eqs 1 and 2 are in agreement with eqs 3 and 4, and 5 and 6. A distinction between the two limiting cases, therefore, must stem from other arguments.

As reported previously,[2-5] all equally 3,5-substituted pyrazole derivatives forming cyclic hydrogen bonded complexes in the solid state present degenerate proton tautomerism. Therefore, the case of DTBUP constitutes the first exception to this finding. Although the pyrazole ring in DTBUP is symmetrically substituted and cyclic dimers are formed, one tautomer is preferentially populated in the solid state. If eqs 3 and 4 were valid, this perturbation should arise from crystal packing effects[19,23] which lower the molecular symmetry; the conformation of the *tert*-butyl groups would, however, not affect the tautomerism. We cannot ignore or exclude this case, but the explanation seems very unlikely. Moreover, the tautomerism exhibits an activation energy of 56.6 kJ mol^{-1} which is substantially higher than the value reported for another dimer, solid 3,5-diphenyl-4-bromopyrazole (DPBrP).[4] As indicated in Table 4, the hydrogen bond distances in both compounds are very similar.

The explanation of the data in terms of eqs 5 and 6 is therefore much more tempting. Here, the tautomerism only takes place in the symmetric dimer AA where it is degenerate (Figure 4). In the other dimers AB and BB which exchange rapidly with AA, the population of the second tautomer would be minimal even in the absence of intermolecular interactions. According to eq 5, the effective energy of activation of the proton transfer is then given by

$$E_{a_{12}} = E_{a_{12}}^{\mathrm{HH}} + \Delta H_{12} \quad (7)$$

Using the value of $\Delta H_{12} = 7.7$ kJ mol^{-1} we obtain

$$E_{a_{12}}^{\mathrm{HH}} = E_{a_{12}} - \Delta H_{12} = (56.6 - 7.7)\mathrm{kJ\ mol^{-1}} \approx 49\ \mathrm{kJ\ mol^{-1}} \quad (8)$$

which is now very close to the value of 44.2 kJ mol^{-1} found for DPBrP.[4]

5. Conclusions

We have shown here that 3,5-di-*tert*-butylpyrazole (DTBUP) is a good example for depicting the complementary relationship between CPMAS-NMR spectroscopy and X-ray crystallography for studying the structures and dynamics of compounds in the solid state. A conformational disorder of the *tert*-butyl groups and of the hydrogen bonded protons of the cyclic DTBUP dimers observed by X-ray crystallography were found by NMR to be dynamic and moderately fast in the NMR timescale. The *tert*-butyl group conformation strongly affects the degeneracy of the intradimer proton tautomerism, particularly when the tautomerism seems to occur only in the symmetric configuration where all *tert*-butyl groups exhibit the same conformation. In the other conformers, the degeneracy of the tautomerism is lifted and the tautomerism suppressed. The observed solid state asymmetry of the tautomerism of DTBUP thus seems to be intrinsic and not induced by solid state interactions. It will be tempting to see whether these results can be confirmed by additional experiments and theoretical calculations.

Acknowledgments. We gratefully acknowledge the European Community [Project SCI 0045.C(H)] and the Fonds der Chemischen Industrie, Frankfurt, for financial support.

JO9319428